PROCEEDINGS OF SCIENCE

Results of the SMILE-2+ balloon experiment

Tomonori Ikeda,[a,*] Atsushi Takada,[a] Mitsuru Abe,[a] Koichiro Kobayashi,[a] Keisuke Tahara,[a] Kei Yoshikawa,[a] Shingo Ogio,[a] Masaya Tsuda,[a] Yura Yoshida,[a] Yoshitaka Mizumura,[b] Takeshi Nakamori,[c] Shunsuke Kurosawa,[d] Tatsuya Sawano,[e] Kenji Hamaguchi,[f] Masaki Mori,[g] Junko Kushida[h] and Toru Tanimori[a]

[a] *Kyoto University, Graduate School of Science, Kitashirakawa Oiwake, Sakyo, Kyoto, Japan*

[b] *Institute of Space and Astronautical Science, Japan Aerospace Exploration Agency Yoshinodai 3-1-1, Chuou, Sagamihara, Kanagawa, Japan*

[c] *Yamagata University, Department of Physics, Kojirakawamachi 1-4-12, Yamagata, Japan*

[d] *Tohoku University, New Industry Creation Hatchery Center, Aoba 6-6-10, Sendai, Japan*

[e] *Kanazawa University, Graduate School of Natural Science and Technology,, Kakuma, Ishikawa, Japan*

[f] *University of Maryland, Department of Physics, Baltimore County 1000 Hilltop Circle, Baltimore, MD 21250, USA*

[g] *Ritsumeikan University, Department of Physics, Noji Higashi 1-1-1, Kusatsu, Japan*

[h] *Tokai University, Department of Physics, Kita-Kaname 4-1-1, Hiratsuka, Japan*

E-mail: ikeda.tomonori.62h@st.kyoto-u.ac.jp

The cosmic MeV gamma-ray observation is a promising diagnostic tool to address the universe. While INTEGRAL and COMPTEL unveiled the MeV gamma-ray sky, the outstanding issue, like the origin of the gamma-ray and positron excesses toward the galactic inner region, remained. Furthermore, the conventional nonlinear imaging with the superposition of the Compton circles and the coded mask aperture system cannot discriminate the background from the signal. To overcome such difficulties, we developed an Electron-Tracking Compton Camera (ETCC), which has a linear imaging system. The balloon experiment on April 2018 in Australia, the so-called SMILE-2+, was carried out, and we observed the galactic diffuse gamma-rays with a significance of 4.3σ in the energy range of 150–600 keV. The gamma-ray flux was consistent with the point-source emission and the annihilation radiation from the positronium observed from INTEGRAL/SPI.

38th International Cosmic Ray Conference (ICRC2023)
26 July - 3 August, 2023
Nagoya, Japan

*Speaker

© Copyright owned by the author(s) under the terms of the Creative Commons Attribution-NonCommercial-NoDerivatives 4.0 International License (CC BY-NC-ND 4.0).

PoS(ICRC2023)663

1. Introduction

Observing the cosmic MeV gamma-ray can reveal various astrophysics phenomena, such as nucleosynthesis, the chemical enrichment of our galaxy [1], and the particle acceleration process of relativistic jets and outflow sources [2]. In particular, the morphology of the annihilation line cannot be explained by conventional astrophysical sources like type Ia supernovae, massive stars, microquasars, and X-ray binaries [3, 4]. The exotic explanations involving dark matter and the primordial black hole are also claimed [5, 6]. Therefore, the precise spectrum and skymap of the cosmic MeV gamma-ray are desired. However, the sensitivity of the MeV gamma-ray observation is modest compared with the X-ray and GeV gamma-ray observations. The main reason is the existence of huge backgrounds such as the atmospheric gamma-rays, the secondary particles produced by the interaction between cosmic-ray particles and instruments, and the activation of radioactive isotopes. Also, conventional Compton cameras don't have the ability to remove such backgrounds.

Therefore, we proposed the sub-MeV/MeV gamma-ray imaging loaded-on-balloon experiment (SMILE) using an electron-tracking Compton camera (ETCC) [7]. The ETCC gives linear imaging of the MeV gamma-ray sky based on geometrical optics owing to recording all information on Compton kinematics, including the direction of the Compton electron [8]. The second balloon experiment, dubbed SMILE-2+, was carried out to observe the Crab Nebula in 2018. We succeeded in detecting with a significance of 4.0σ in the energy range 0.15–2.1 MeV [9]. In addition, we observed the galactic center region for three hours before starting discharge in the gas detector. In this paper, we present results from the analysis of the galactic center region obtained with the SMILE-2+ experiment.

2. SMILE-2+ experiment

The SMILE-2+ experiment was conducted in Alice Springs on April 7, 2018. The balloon floated at 37.8–40.4 km altitude, corresponding to an atmospheric depth of 2.4–3.9 g/cm^2. The total duration was approximately 26 h. The Crab Nebula and the galactic center entered the field of view of the ETCC detector during the observation.

The ETCC detector consists of a gas time projection chamber (TPC) and pixel scintillator arrays (PSAs), which are assigned as Compton-scattering targets and absorbers of scattering gamma-ray. The detection volume of the TPC is $30 \times 30 \times 30$ cm^3 and filled in an argon-based gas (95%Ar + 3%CF_4 + 2%iso-C_4H_{10}) at 2 atm. The 108 PSAs are arranged at the bottom and side of the TPC. Each PSA is made of GSO (Gd_2SiO_5:Ce) scintillators of 8×8 pixels with a pixel size of 6×6 mm^2. The thicknesses of the side and bottom scintillator are 13 mm and 26 mm, respectively. The effective area of the ETCC detector is largest at the zenith direction, which is 0.3 cm^2 to the gamma-ray of 662 keV. The field of view is defined as the zenith angle, the half-effective area of the zenith direction, and corresponds to 3.1 sr. More description is found in Ref [9]. The point spread function of the ETCC comprises the angular resolution measure (ARM) and the scattering plane deviation (SPD) [8]. The ARM and SPD are the determination accuracy of the Compton scattering angle and the angular ambiguity along the Compton circle. The FWHM value of ARM and SPD at 662 keV are 10.5 and 50 degrees, respectively, then the point spread function evaluated by the half-power radius reaches 20 degrees [10].

PoS(ICRC2023)663

3. Result of the galactic center

We select the high-altitude data from 9:00 ACST (Australian Central Standard Time) on April 7 to 6:30 ACST on April 8. The observed skymap is shown in Figure refskymap(a) and strongly correlates with the exposure. The one pixel of the skymap corresponds to 1 sr. The background gamma rays consist of the extragalactic, atmospheric gamma rays, and induced gamma rays by the interaction between instruments and cosmic rays or secondary particles. The flux of extragalactic gamma rays is affected by the atmospheric depth owing to atmospheric absorption. Also, the flux of atmospheric gamma rays correlates with the atmospheric depth owing to atmospheric absorption and production. This correlation is known as the growth curve [11]. We made the growth curve depending on gamma-ray energy and calculated the correlation factors between the detected intensity and the atmospheric depth via fitting by the empirical function. In addition, we made the background skymap on the detector coordinate by accumulating observed events except for the data, including the galactic center. The uncertainty of the fitting parameter and the statistic error of the background skymap are treated as systematic errors. The skymap of the background model and the differential map are shown in Figure 1(b) and 1(c), respectively. We found the excess in the galactic center. It should be noted that this skymap did not indicate a true MeV gamma-ray sky because we did not take into account the response function.

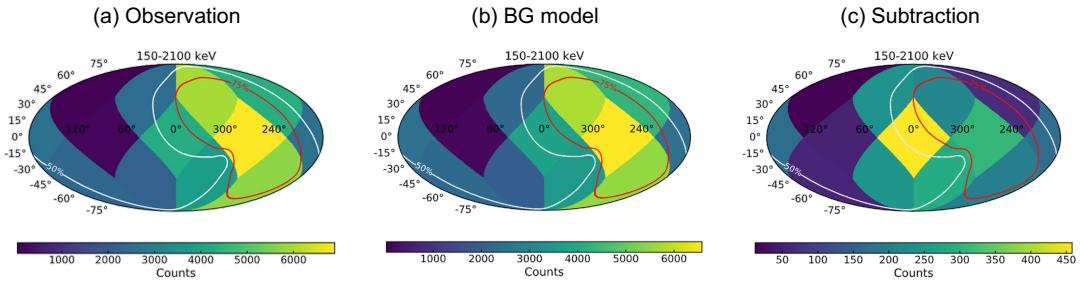

Figure 1: Skymap of (a) the high-altitude data and (b) the background model in the galactic coordinate. (c) Differential skymap of the observation and the background model. The red and white lines indicate the 75% and 50% exposure area, respectively.

The energy spectrum of the observation data and background model on the pixel of the galactic center is shown in Figure 2(a). The blue points and errors, including statistics and systematic, denote the subtraction spectrum. We detected the excess with the significance of 4.3σ. The systematic error comes from the uncertainty of the background model.

We calculated the flux of the galactic center region in the energy range of 150–600 keV. Because of the low statistic of the observation data, deriving the full-sky emission morphology is delicate. Thus, we fixed the point-source fluxes and distribution using the INTEGRAL source catalog [12]. In addition, the morphology of galactic annihilation emission of Siegert's model [4], which consists of the Galaxy's center, the narrow and broad bulge, and the low surface brightness disk, was used. The observation image was divided into 12 pixels, and each pixel has four energy bins in the range of 150–600 keV. The pixel number and energy bin are denoted as p' and e', respectively. The

PoS(ICRC2023)663

expected number $m^{p',e'}$ is written as,

$$m^{p',e'} = \sum_{t} \sum_{p=0}^{p=12} \sum_{e=0}^{e=4} R_{t,p,e}^{p',e'} (\theta^{p,e} M^{p,e} + P^{p,e}) + \sum_{t} \phi_t^{e'} B_t^{p'}, \quad (1)$$

where e, p, and t describe the unfolding energy bin, the pixel number of the unfolding emission map, and the observation time, respectively. $R_{t,p,e}^{p',e'}$ is the response function of the ETCC detector. $\theta_{p,e}$, $M_{p,e}$, and $P_{p,e}$ are unfolding energy flux, the skymap of Siegert's model, and the emission model of the point sources. $\phi_t^{E'}$ is the background rate correlated with the atmospheric depth and $B_t^{p'}$ represents the emission map of estimated background. We evaluated $\theta^{p,e}$ using the least χ^2 square method. The fitting and unfolding spectrum are shown in Figure 2(b) and 2(c). The minimum χ^2/NDF value was 40/44. Also, we compared the observed light curve with the expected one using the obtained parameter in Figure 3.

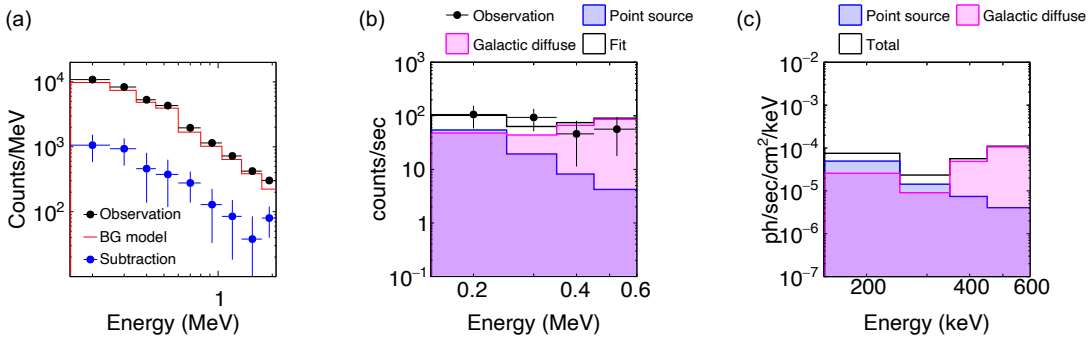

Figure 2: (a) Energy spectrum of the galactic center. The black points and red line indicate the observation data and the background model, respectively. The blue points are the subtraction spectrum. The errors include systematic uncertainty. (b) Fitting spectra of the galactic center in the 0.15–0.6 MeV. The black points and the black line denote the observation data and fitting spectrum. The blue and magenta histograms are contributions of the point sources and the galactic diffuse emission. (c) Unfolding spectrum of the galactic center. The blue and magenta are contributions of the point sources and the galactic diffuse emission.

4. Discussion

We compare our measured intensity with other experiments in Figure 4. Our result is in agreement with that of INTEGRAL/SPI [13, 14]. However, the energy region of 150–300 keV is discrepant. In such energy regions, the cosmic diffuse gamma-ray consists of the inverse Compton, stellar emission, and annihilation emission from INTEGRAL's results [13]. Our analysis did not consider the morphology of the stellar emission and inverse Compton in the low-energy region. Hence, we have concluded that the best-fit spectrum converged to explain the emission of 300–600 keV, so the spectrum of 150–300 keV was misaligned with the INTEGRAL' result.

Acknowledgements

This study was supported by Japan Society for the Promotion of Science (JSPS) KAKENHI Grant-in-Aids for Scientific Research (Grant Numbers 21224005, 20244026, 16H02185, 15K17608,

PoS(ICRC2023)663

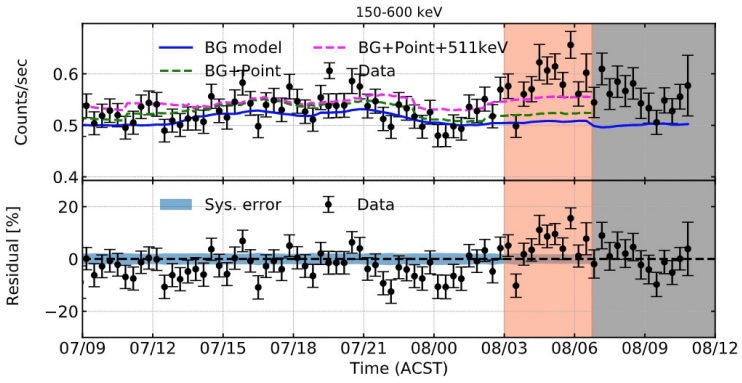

Figure 3: Top panel shows the comparison of the light curve in the field of view. The black points are the observation data. The blue solid, green dashed, and magenta dashed lines denote contributions of the background model, the point sources, and the galactic diffuse emission, respectively. The bottom panel indicates the differential light curve. The blue band presents systematic uncertainty.

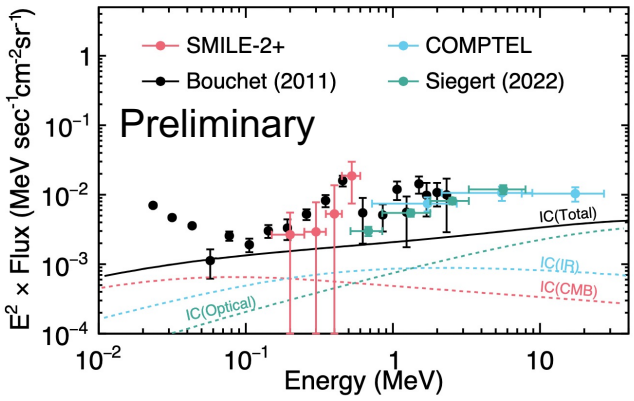

Figure 4: Spectrum of the diffuse emission in the galactic center region. The red points are the SMILE-2+ result. The black and green points are the low and high energy results of INTEGRAL/SPI [13, 14]. The blue points are for COMPTEL [15]. The red, blue, and green dashed lines are IC components as modeled on the CMB, on the diffuse IR, and on the diffuse optical [16].

23654067, 25610042, 16K13785, 20K20428, 16J08498, 18J20107, 19J11323, and 22J00064), a Grant-in-Aid from the Global COE program "Next Generation Physics, Spun from Universality and Emergence" from the Ministry of Education, Culture, Sports, Science and Technology (MEXT) of Japan, and the joint research program of the Institute for Cosmic Ray Research (ICRR), The University of Tokyo. The balloon-borne experiment was conducted by Scientific Ballooning (DAIKIKYU) Research and Operation Group, ISAS, JAXA. Some of the electronics development was supported by KEK-DTP and Open-It Consortium.

PoS(ICRC2023)663

References

[1] R. Diehl, *Reports on Progress in Physics*, **76** (2013) 026301.

[2] M. Chiaberge, A. Capetti and A. Celotti, *Monthly Notices of the Royal Astronomical Society* **324** (2001) L33–L37.

[3] N. Prantzos, et al., *Rev. Mod. Phys.*, **83** (2011) 1001–1056.

[4] T. Siegert, R. Diehl, G. Khachatryan, M. G. H. Krause, F. Guglielmetti, J. Greiner, A. W. Strong and X. Zhang, *A&A* **586** (2016) A84.

[5] P. Sizun, M. Cassé and S. Schanne, *Phys. Rev. D* **74** (2006) 063514.

[6] R. Laha, *Phys. Rev. Lett.* **123** (2019) 251101.

[7] T. Tanimori, et al., *The Astrophysical Journal* **810** (2015) 28.

[8] T. Tanimori, et al., *Sci. Rep.* **7** (2017) 41511.

[9] A. Takada, et al., *The Astrophysical Journal* **930** (2022) 6.

[10] T. Ikeda, et al., *Prog. Theor. Exp. Phys.* **8** (2021) 083F01.

[11] V. Schönfelder, U. Graser, and J. Daugherty, *The Astrophysical Journal* **217** (1997) 306-319.

[12] L. Bouchet, et al., *The Astrophysical Journal* **679** (2008) 1315-1326.

[13] L. Bouchet, et al., *The Astrophysical Journal* **739** (2011) 29.

[14] T. Siegert, et al., *Astronomy & Astrophysics* **660** (2022) A130.

[15] A.W. Strong, et al., *Astron. & Astrophys. Suppl. Ser.* **120** (1996) 381-387.

[16] E. Orlando, *MNRAS* **475** (2018) 2724-2742.

PoS(ICRC2023)663